Importance of Capillary Forces in the Assembly of Carbon Nanotubes in a Polymer Colloid Lattice

Izabela Jurewicz, Joseph L. Keddie and Alan B. Dalton*

Department of Physics, Faculty of Engineering & Physical Sciences, University of Surrey, Guildford,

GU2 7XH, UK

*E-mail: a.dalton@surrey.ac.uk

We highlight the significance of capillary pressure in the directed assembly of nanorods in ordered arrays of colloidal particles. Specifically, we discuss mechanisms for the assembly of carbon nanotubes at the interstitial sites between latex polymer particles during composite film formation. Our study points to general design rules to be considered to optimize the ordering of nanostructures within such polymer matrices. In particular, gaining an understanding of the role of capillary forces is critical. Using a combination of electron microscopy and atomic force microscopy, we show that the capillary forces acting on the latex particles during the drying process are sufficient to bend carbon nanotubes. The extent of bending depends on the flexural rigidity of the carbon nanotubes and whether or not they are present as bundled ensembles. We also show that in order to achieve long-range ordering of the nanotubes templated by the polymer matrix, it is necessary for the polymer to be sufficiently mobile to ensure that the nanotubes are frozen into the ordered network when the film is formed and the capillary forces are no longer dominant. In our system, the polymer is plasticized by the addition of surfactant, so that it is sufficiently mobile at room temperature. Interestingly, the carbon nanotubes effectively act as localized pressure sensors and, as such, the study experimentally verifies theoretical predictions that the

emergence of capillary forces during the latex films formation is greater than approximately 10^{-8} N.

1. Introduction

Self-assembly, particularly prevalent in natural materials, is a promising tool to bottom-up formation of nanostructures with controlled architectures. There are many elegant examples found in nature where controlled self-assembly has produced hierarchical materials with extraordinarily complex geometries, both in two-dimensional (2D) lattices and three-dimensional (3D) crystals. The majority of these processes are driven by capillary forces arising from the intermolecular attraction between liquid and solid materials. [1, 2] Mimicking these processes in synthetic systems has proven most challenging. However, there are examples whereby directed self-assembly[3] has been successfully used for the formation of relatively complex structures using metal particles[4, 5], nanorods[6], carbon nanotubes (CNTs)[7-10] and more recently graphene[3, 11, 12].

Due to a combination of excellent physical and chemical properties, CNTs, in particular, have been among the most studied materials for the past two decades. During that time, several potential applications have emerged, such as field-emission displays[13], field-effect transistors[14], sensors[15] and photonic devices[16, 17]. In particular, their use as active fillers in polymer composites has proved promising by imparting both enhanced electrical and mechanical functionality. However, a major obstacle delaying deployment of composites and devices containing CNTs at an industrial scale is the problem of achieving controlled and homogeneous dispersion or assembly of CNTs within a polymer matrix.

As-produced CNTs have the tendency to assemble into ropes due to the strong van der Waal's interactions between them. Their large surface area and high degree of entanglement can be responsible for detrimental formation of agglomerates when mixed with a polymer. Pristine nanotubes are also extremely hydrophobic and are insoluble in most organic and aqueous solvents.

Thus, in order to achieve high production capacities of CNT-based polymer composites in a commercially viable manner, it is necessary to develop a strategy for assembling CNTs reproducibly,

controllably and with high-throughput. In terms of nanocomposites, the precise control of CNT distribution, orientation and bundle size within the polymer matrix is a critical prerequisite toward future technological applications. A homogeneous distribution of CNTs also ensures the achievement of maximum interfacial area between CNTs and the polymer matrix, which may facilitate, for instance, improvement of interfacial stress transfer for mechanical applications.[18, 19] Therefore, greater efforts are required to disperse nanotubes in polymers and other hosts.

One of the promising approaches to controlled assembly is the use of colloidal templating. This has already proven successful for a range of applications from inverse-opal photonic crystals[20, 21] to high surface area sensors.[22] Self-assembly of colloidal particles is an effective strategy for fabrication of ordered nanostructures. Polymers can be synthesized as mono-size particles in water and their inherent properties (stemming from crosslinking, chain branching and glass transition temperature), as well as surface chemical composition, can be easily adjusted during the emulsion polymerization process. Moreover, the particle surface can be modified by the addition of additives that adsorb at the interface with water.[23]

Recently there have been several reports of self-assembly of CNTs into 2D and 3D geometries using colloidal crystals based on polymer templates. Liu *et al.*[24] showed that it is possible to selectively self-assemble surface-functionalized double-wall carbon nanotubes (DWNT) in block copolymer templates as well as to template amino-functionalized multi-walled CNTs over sacrificial polystyrene (PS) sulfate latex particles.[25] A polyelectrolyte-assisted layer-by-layer (LbL) technique has also been used to deposit CNTs on silica, polystyrene, and melamine spherical colloids of different sizes.[26]

Another effective way of tuning and manipulating a polymer-nanoparticle interface is through the non-covalent functionalization of CNTs with surfactants or polymers. In an early example, Grunlan *et al.*[27] used highly amphiphilic and charged molecules of gum arabic (GA) to provide steric stabilisation reinforced by electrostatic repulsion for single-wall carbon nanotubes (SWNT)s embedded in a poly(vinyl acetate) (PVAc) matrix. As we have recently shown, [28, 29] CNTs stabilised by a non-ionic

surfactant can be successfully assembled into highly-ordered structures utilizing a polymer colloidal crystal template.

Here, we study the influence of capillary forces combined with a physical template (colloidal template) as a way to drive the self-assembly of CNTs into highly ordered structures. We also investigate the influence of the extent of plasticization of the polymer particles and the flexural rigidity of CNTs on the level of self-assembly and the local nanoscale morphology of the composite material. The results point to some general guidelines that must be considered more generally for the controlled design of colloidal-based composite systems containing any nanostructured filler.

2. Materials and Methods

2.1. Materials

Single-wall carbon nanotubes (SWNTs) synthesized through high-pressure catalytic decomposition of carbon monoxide (HiPCO) were purchased from CNI Nanotechnologies, TX, USA. Multi-wall carbon nanotubes (MWNTs) and double-wall carbon nanotubes (DWNTs) were purchased from Nanocyl S.A.

The latex polymer used as the template for CNT assembly, provided by DSM NeoResins (Waalwijk, The Netherlands) is based on a random copolymer of butyl acrylate (BA), methyl methacrylate (MMA) and methacrylic acid (MAA) in a molar ratio of BA:MMA:MAA of 85:10:5, as described elsewhere.[30]. The polymer particle size is 270 nm, its dry glass transition temperature (T_g) is 28 °C, and the initial solids content is 49.5 wt.%. The latex dispersion was prepared by semi-batch emulsion polymerization using sodium dodecyl sulfate (SDS) to achieve stability and ammonium persulfate as the initiating salt.[30]

2.2. Preparation of aqueous dispersions of CNTs

As-received SWNTs were dispersed in deionised water, containing either 1 wt. % (1) non-ionic surfactant, Triton X-100 (Fisher Scientific); (2) anionic surfactant, sodium dodecyl sulfate, SDS (Fisher Scientific); or cationic surfactant, cetyltrimethylammonium bromide, CTAB (Fisher Scientific). The

dispersions were sonicated using a probe ultrasonicator (Branson Sonifier, model 150D) for 20 minutes at a power level of 20 Watts in an ice-cold water bath resulting in the CNT concentrations in water as high as 1 mg ml^{-1}. MWNTs and DWNTs were dispersed and exfoliated following the same procedure as just described for SWNTs. Nine different CNT dispersions were prepared in total (three different types of CNTs and three different types of surfactants).

2.3. Preparation of composites

Each of the aqueous CNT-surfactant dispersions were then blended with the latex by stirring, thus resulting in nine different types of dispersions. The latex-SWNT mixtures were sonicated in an ice-cold water bath for 10 minutes. The final weight fraction of CNTs in all dispersions was 0.5 wt. % based on the solids content of polymer latex in the dispersion (determined by TGA). All nine composite dispersions were deposited onto poly(tetrafluoroethylene) (PTFE) moulds by drop casting and subsequently left to dry for 48 hours at room temperature (~21 °C).

2.4. Characterization

Microstructural investigations of composite materials were made using a Hitachi S-4000 scanning electron microscope (SEM) at an accelerating voltage of 10-15 kV, a working distance of 6-10 mm, and a spot size of 5 nm. Owing to the relatively high electrical conductivity of the samples, they were imaged without sputtering a metal onto their surface. For topographic studies, an atomic force microscope (AFM) (NT-MDT, Moscow, Russia), using semi-contact mode, was employed. The AFM probes (NT-MDT) had an average spring constant of 11.8 N/m. The T_g of the original polymer latex and all composites was determined using a differential scanning calorimeter (DSC) (TA Instruments Q1000, New Castle, USA). A standard heating rate of 10 °C/min, and cooling rate of 20 °C/min were used for all samples. The value of T_g was taken in the second heating scan at the midpoint step-wise increase of the specific heat associated with glass transition.

3. Results

This study aims to explain the forces and factors that influence the self-assembly of CNTs in colloidal crystals. The interface between CNTs and polymers in colloidal composites were modified through variation of the surfactant used to stabilize the nanotube dispersion in the initial liquid state. For this purpose, aqueous dispersions of SWNTs, MWNTs and DWNTs were prepared using three surfactants of differing charge: a) a non-ionic surfactant, octyl-phenol-ethoxylate (Triton X-100), b) an anionic surfactant, sodium dodecyl sulphate (SDS), and c) a cationic surfactant, cetyltrimethylammonium bromide (CTAB).

In order to study the extent of ordering of CNTs at the polymer particle interface, SEM analysis of the nanocomposite surfaces was employed, and the results are shown in Figure 1a-g. As can be seen in Figure 1a, when utilizing Triton X-100, SWNTs have self-assembled into a honeycomb-like structure templated by the hexagonal close-packed (HCP) particle arrangement in the colloidal crystal. The diameter of the ring-like structure of CNTs corresponds to the polymer particle size. The CNTs have clearly wrapped around each particle. The ordering is three-dimensional and highly controlled, as was shown elsewhere[28]. Changing the type of CNTs from SWNTs to MWNTs also produces self-organized HCP arrangements (Figure 1b), however the structure is slightly less perfect. Finally, the DWNTs also exhibit structural ordering in the nanocomposite, however they appear to be more rigid and to form a 'snake-like' configuration between the latex particles, as is shown in Figure 1c.

Next we consider the effect of surfactant type. By replacing the Triton X-100 with the anionic surfactant SDS, the microstructure of the nanocomposite is completely modified. As is shown in Figure 1d and 1e, despite the fact that both SWNTs and MWNTs appear uniformly distributed within the latex particle matrix, no apparent ordering of the CNTs is seen. Moreover, in the case of composites containing DWNTs, shown in Figure 1f, the CNTs act as semi-rigid rods distributed between polymer particles in a snake-like manner.

When CTAB-stabilised CNTs were introduced into the latex, a marked increase in the dispersion

viscosity occurred, and a gel was formed. For that reason it was not possible to obtain a smooth composite film. Figure 1g shows the drop-cast sample with SWNTs randomly distributed within the polymer matrix. Due to the inability to form films containing CTAB, the characterisation of composites containing other types of CNTs was not carried out. With CTAB, the dispersed CNTs develop a positive charge. As the latex particles are negatively charged, it is likely that the CNTs were attracted to the polymer particles and bridged particles. This type of flocculation explains the increase in the viscosity and the resulting disordered structures.
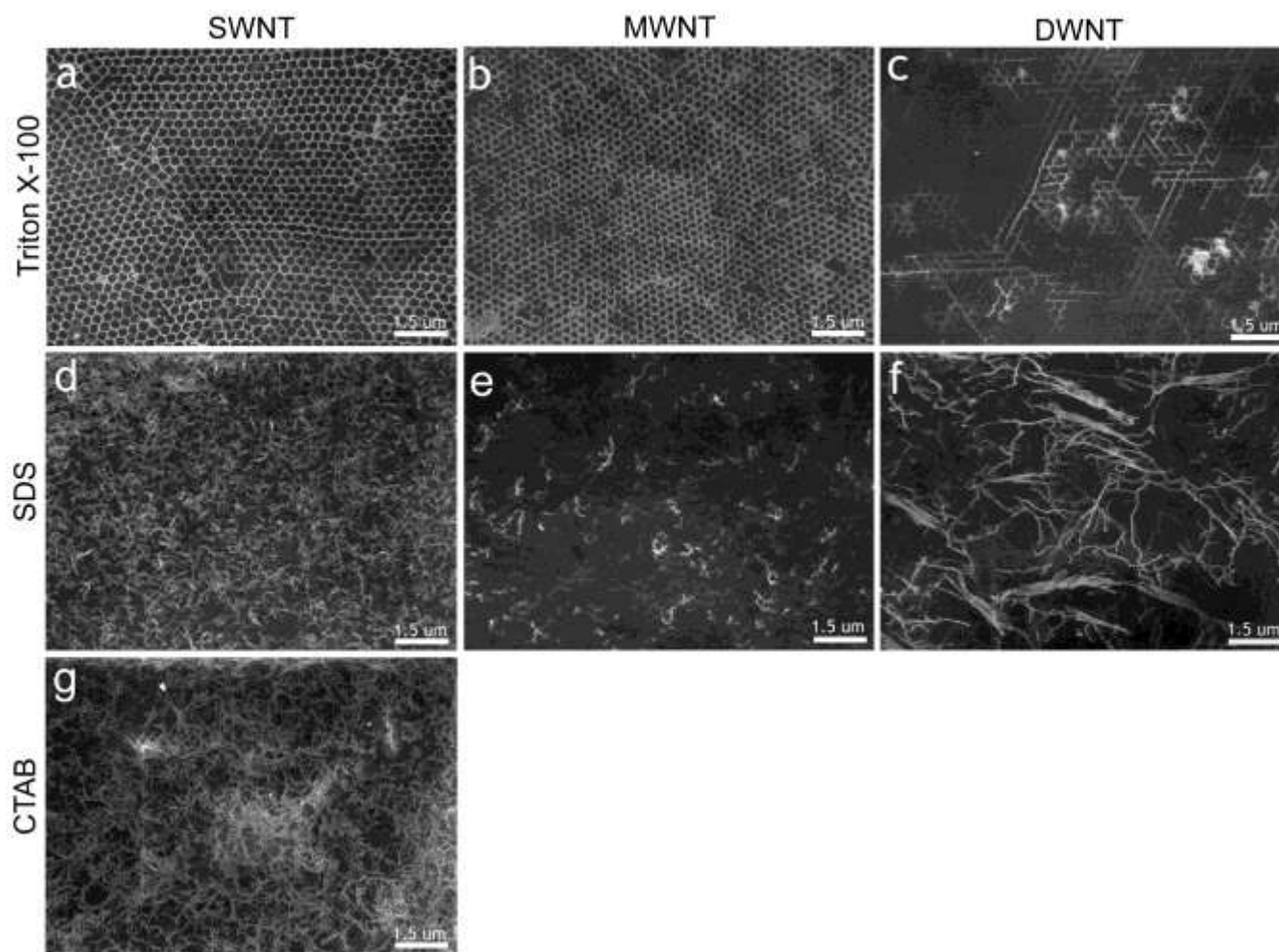

Figure. 1. SEM micrographs of latex composites containing various types of CNTs stabilized with surfactants of different headgroup charge. Latex composites containing a non-ionic surfactant (Triton X-100) and (a) SWNT, (b) MWNT and (c) DWNT; latex composites containing an anionic surfactant (SDS) and (d) SWNT, (e) MWNT and (f) DWNT; latex composite containing a cationic surfactant

CTAB and (g) SWNT. All composites prepared for this study contain 0.5 wt. % CNTs.

To examine further the modifications to the nanocomposite's nanostructural ordering, pattern recognition analysis of representative SEM images was performed using the fast Fourier transformation [FFT] method. The Fourier transform of a lattice containing periodic networks of CNTs perfectly templated by close-packed spherical particles will consist of a series of points whose symmetry of positions is related to those of the lattice points and whose intensity is modulated by sampling by the Airy diffraction pattern associated with each CNT-wrapped particle. The presence of such spots is a direct indication that a high degree of ordering exists. The distance of the spots from the FFT image center is inversely related to their spacing in real space.

Figure 2 shows the frequency-domain patterns generated by 2D FFT analysis of the micrographs. For composites containing SWNTs and MWNTs prepared using Triton-X100, the composites exhibit long-range hexagonal structural order, which is indicated by a series of six bright spots with six-fold rotational symmetry in the resulting FFT spectra shown in Figure 2(a,b). Close inspection of these patterns indicates that there is an apparent broadening of the spots, which results from the presence of hexagonal domains with different orientation within the sample. The FFT spectrum of the composite containing DWNT prepared using Triton-X-100, shown in Figure 2c, exhibits marked broadening and reduced intensity of the lattice-derived spots and increased intensity of the central Airy disc, indicating that the lattice ordering of the nanotubes is reduced. As the ordering of the nanotubes by the lattice is reduced further through preparation of composites with SDS or CTAB (Figure 2d to 2g), the presence of points due to regular ordering diminishes, and the FFT spectrum is indicative of a disordered array of lattice points, characterized by a broad, intense Airy disc at the centre of the pattern. It is interesting to note that the FFT spectrum associated with the DWNT composite prepared using SDS, shown in Figure 3f, appears stretched in one direction and squeezed in the other.
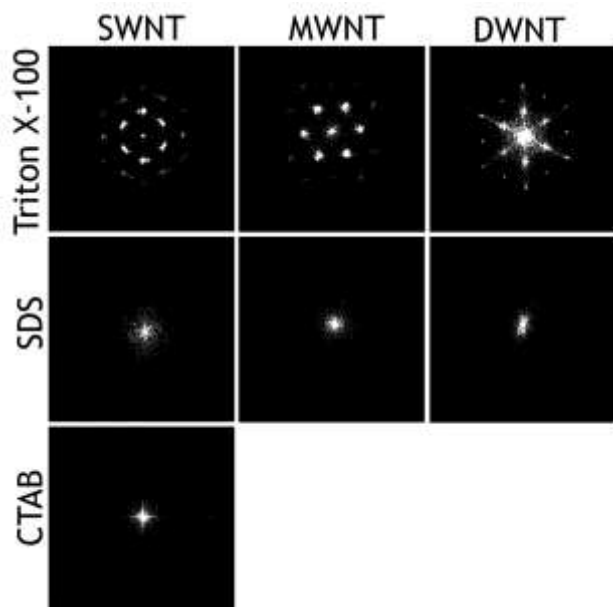
Figure 2. The frequency domain patterns generated by 2D FFT analysis of SEM micrographs presented in Figure 1 for latex composites containing a non-ionic surfactant (Triton X-100) and (a) SWNT, (b) MWNT and (c) DWNT; latex composites containing an anionic surfactant (SDS) and (d) SWNT, (e) MWNT and (f) DWNT; latex composite containing a cationic surfactant CTAB and (g) SWNT.

4. Discussion

There are two main trends that we need to explain. Firstly, there are differences in the extent of structural ordering of CNTs which depend on whether the surfactant is Triton X-100, SDS or CTAB. Secondly, there are differences observed when comparing the composites fabricated using the different type of CNTs (SWNTs, MWNTs, and DWNTs).

From our observations, the surface charge of the latex particles and the post-added surfactant type play important roles in the self-assembly of CNTs. When a surfactant is miscible with a polymer matrix, it can act as a traditional plasticizer and reduce the glass transition temperature.[31, 32] Surfactants can also plasticize the outer regions of polymer particles, to create a shell structure.[33] In all the composites studied here, any excess surfactant that is not adsorbed on the CNT surface will be contained in the

interstitial voids between the latex particles in the form of free surfactant.[34] We hypothesize that in our case, the surfactant could plasticize the polymer particles and facilitate the formation of long range honeycomb-like ordering of CNTs. Additional experiments tested this hypothesis. Below, we separate our discussion into three distinct sections. Firstly, we discuss the role of surfactant in plasticizing the latex particles. Secondly, we discuss the emergence of capillary forces that may act locally at interfaces between particles during composite film formation. Finally, we relate the emergence of these capillary forces to the propensity of CNTs to bend effectively around polymer particles and as a result form extended honeycomb networks.

4.1. Particle plasticization by surfactants

To investigate the extent of plasticization by the three types of surfactant, DSC was performed. The results are shown in Figure 3a. The T_g of the original latex was measured to be 28 °C. Composites containing Triton X-100 and all types of CNTs show a significant reduction of T_g. In the case of SWNTs, the T_g is reduced to 19 °C, and for MWNTs and DWNTs, it is reduced to 24 °C and 24.5 °C, respectively. To determine whether this substantial decrease in T_g can be attributed to the presence of surfactant rather than to the direct effect of CNT incorporation, a control experiment was conducted. The same amount of Triton X-100 was added to the latex as was added with the CNTs in the composite. A decrease in T_g by 10 °C was observed, indicating that the free surfactant is indeed plasticizing the polymer matrix.
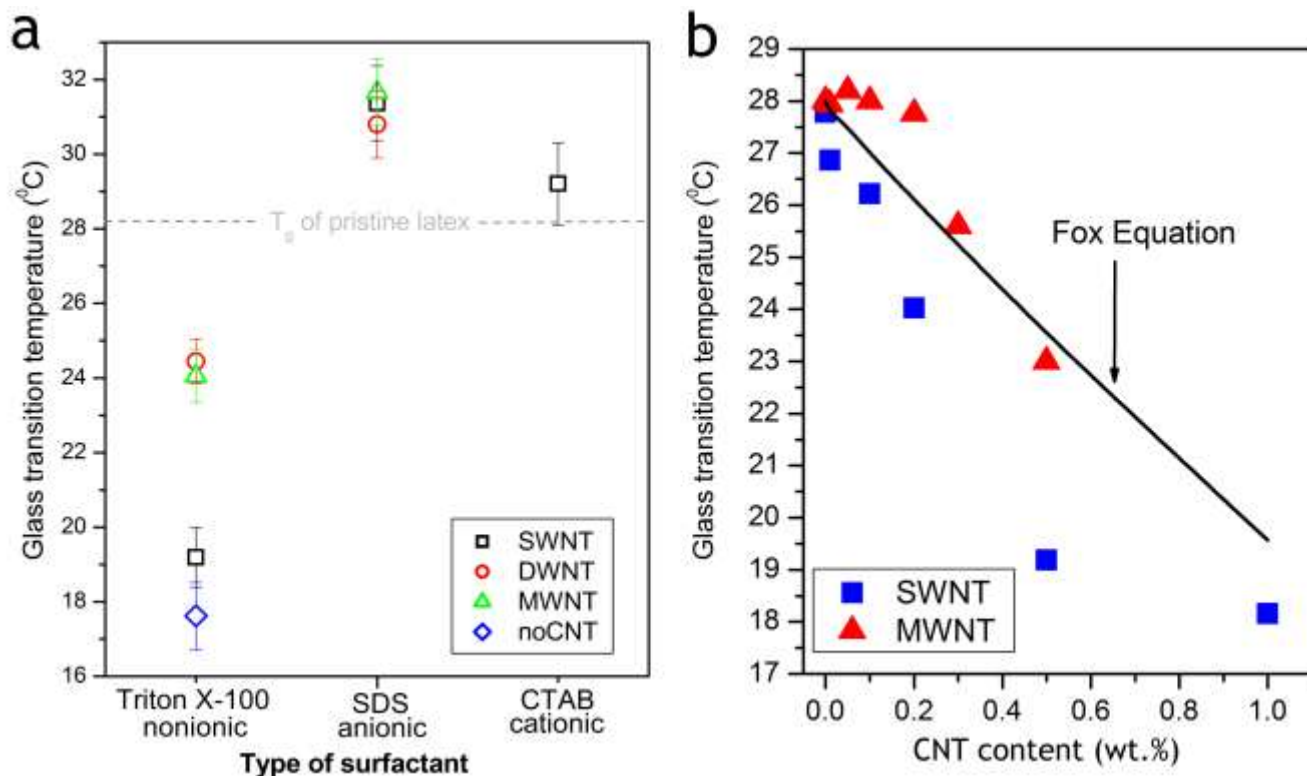
Figure 3. (a) The change in the T_g of the original latex and latex nanocomposites containing 0.5 wt.% SWNTs, MWNTs and DWNTs as a function of the type of post-added surfactant. (b) The change in T_g as a function of concentration of non-ionic surfactant (Triton X-100) stabilized CNTs: (■) SWNT and (▲) MWNT. The solid line is a prediction of T_g utilizing the Fox equation (for the situation where all of the surfactant takes part in the plasticization of the polymer latex).

Interestingly, there is a noticeable difference in the T_g between composites containing Triton X-100 stabilised SWNTs and those containing MWNT and DWNTs. We hypothesize that this is due to the fact that the surface area of CNTs accessible to the surfactant molecules varies for the different forms of CNTs.[35] The surface area per unit volume ratio (S/V) of SWNT bundles is relatively smaller than the S/V of individual de-bundled MWNTs and DWNTs. Therefore, in the case of SWNTs, less surfactant molecules can be adsorbed on the nanotube surface and consequently non-adsorbed surfactant can plasticize the polymer, as shown in Figure 3b. Additionally, owing to the composite fabrication method, if more CNTs are introduced into the polymer, more surfactant is present in the composite. As a result

of the larger S/V, greater amounts of Triton X-100 are adsorbed on the MWNT surface, and less surfactant is available to plasticize the polymer phase when compared with the composite containing SWNTs.

It is well known that the presence of low molecular weight additives, such as surfactants, can markedly increases the free volume of a polymer and subsequently lower the T_g. The observed plasticization can be described by the Fox equation[36] and is defined in Equation 1 below:

$$\frac{1}{T_g} = \left(\frac{x_{surf}}{T_{g,surf}} + \frac{x_{polymer}}{T_{g,polymer}} \right) \tag{1}$$

where T_g is the predicted glass transition temperature resulting from plasticisation, x_{surf} is the weight fraction of the surfactant, $T_{g,surf}$ is the glass transition temperature of the pristine polymer, $x_{polymer}$ is the weight fraction of polymer, and $T_{g,polymer}$ is the glass transition temperature of the pristine polymer.

This equation is plotted for different weight concentrations of CNTs as the solid line in Figure 3b. The actual weight fractions of the polymer and surfactant used to prepare the composites containing SWNT/Triton X-100 and MWNT/Triton X-100 were used in the calculations. In this calculation, it was assumed that all of the surfactant desorbed from the CNTs and plasticized the polymer. A T_g value of 28 °C (measured by DSC) was used for the dried original polymer, and a T_g of -61°C (determined independently by DSC) was used for Triton X-100.

It should be noted that the predicted T_g is only for the situation where all of the surfactant takes part in the plasticization of the polymer latex. Of course, in reality, as some of the Triton X-100 is adsorbed on the CNT surface, the effective wt. % causing plasticization is reduced unless desorption is complete. As can be seen in Figure 3b, the dependence of the experimental T_g of the composite as a function of wt. % of MWNTs is markedly different to that predicted by the Fox equation with higher values predicted for specific weight fractions of CNTs. Only at higher MWNT concentrations (0.5 wt. % and above) the

experimental T_g values become lower than the predicted value. For the composite containing SWNTs and Triton X-100, a significantly lower T_g is obtained compared to the predicted T_g at different weight fractions. It should be noted that polymers produced by emulsion polymerization can be saturated with water. [37, 38] Hydroplasticization (plasticization by water) can reduce the T_g of the polymer as a result of the specific interaction of water molecules.[39] Although the polymer in the dry state no longer contains water, it is possible that the polymer contains water when dispersed as particles in the wet latex. Thus, it is possible that the lowering of the T_g of polymer composites is associated with both the plasticizing effect of the surfactant combined with hydroplasticization. Comparison to the Fox equation prediction confirms that the surfactant on the MWNTs does not plasticize the polymer until there is a higher concentration. This result can be associated with the higher surface area (compared to SWNTs), which adsorbs more surfactant before an excess is reached and plasticization begins.

As is shown in Figure 3a, the composites containing SDS, regardless of the type of CNTs added, show an increase in T_g by 3 °C compared to the pristine polymer latex. The increase in T_g (anti-plasticization) can be explained as follows. The polymer latex contains hydrophilic carboxylic acid monomers (such as MAA) that are commonly added to synthetic latices to alter the polarity of the polymer latex as well as the interactions that arise between the polymer and the surfactant and most importantly to provide colloidal stability.[40, 41] Therefore, the presence of acidic groups at the interface increases hydrophilic interactions between the polymer surface and the SDS molecules. In the latex dispersion, the alkyl chain of the surfactant molecule associates with the hydrophobic regions of the latex surface and the charge group orientates itself toward the aqueous solution. When combining dispersions, more SDS surfactant is likewise introduced. With increasing SDS concentration introduced at the interface, the surfactant molecules relocate and align perpendicular to the surface producing a more compact coverage.[42, 43] The overall T_g of the composite is increased compared to the T_g of the pristine polymer latex.

Introducing the cationic surfactant CTAB to the negatively-charged dispersion induces latex

coagulation. The mechanism of coagulation is derived from the positively-charged CTAB neutralising the opposite charges on the particles (charge neutralisation). Consequently, bridging flocculation is enabled by the reduction in the electric double layer repulsion between particles.[44, 45] In the composite, part of the cationic surfactant is adsorbed on the CNT surface, thus the bridging may take place between latex particles and CNTs. No change in the T_g was observed for this system.

Due to issues with film formation when using CTAB, the following discussion will only concentrate on the comparison of the composites containing Triton X-100 and SDS surfactants. From now on, we shall simplify the discussion by referring to the composite containing non-ionic surfactant (Triton X-100) as "plasticized composite", and latex particles plasticized by this surfactant as "plasticized particles". We shall call the composite containing anionic surfactant (SDS) "unplasticized composite," and particles unaffected by this surfactant are called "unplasticized particles".

4.2. The role of capillary forces on compaction and deformation of latex particles

In order to understand why the CNTs bend and deform into continuous networks around the latex spheres, it is necessary to analyze the deformation of polymer particles and forces active during the film formation process. In the first stage of drying, the nanocomposite dispersion is deposited onto a substrate. Water evaporates resulting in a decreased average interparticle spacing as particles are forced into a close-packed array. At this stage the particles remain spherical and undeformed. In the second stage, as water continues to evaporate, the water-air (w/a) interface recedes into the surface pores creating a differential capillary pressure. As a result of the efficient particle wetting, the resulting interface takes up on a curved meniscus, with air being on the inner side of the curvature. The resulting capillary force exerted by the top layer of particles on the particles below causes them to deform. Since the pressure differential across the meniscus is inversely proportional to its radius of curvature, a smaller radius of curvature will result in greater capillary pressure.[46] With progressive drying, some water is left at the contacts between the particles forming liquid bridges. For a concave

liquid bridge, a negative capillary force is generated that will further press the particles together, leading to the elimination of interstitial voids, the extent depending on the viscoelastic properties of the polymer. (Particles at temperatures near to their glass transition temperature will undergo minimal deformation under capillary forces but rather undergo slower deformation driven by reduction of the polymer/air interfacial energy.) Finally, particles undergo coalescence through the interdiffusion of polymer molecules, eventually forming a continuous film.

Visschers et al. calculated the forces needed for successful deformation of particles[47] and derived an equation to describe the dominant capillary driving force, which is due to the receding w/a interface (eq. 2)[47]:

$$\frac{Fc_{w/a}}{\gamma_{w/a} r_p \cos\theta} = \frac{2\sqrt{2}(1-f)^2}{\frac{2}{3}\sqrt{3}-1} \tag{2}$$

where γ is the w/a surface tension, r_p is the particle radius, θ is the contact angle measured through the liquid, and f is the extent of deformation (f = 0 for absence, and f = 0.095 in the presence of maximum particle deformation). Using eq. 2 and data listed in Table S1 (Supporting Information), we have calculated the capillary forces resulting from the receding w/a interface for our system to be ~10^{-7} N, which is of the same order of magnitude reported elsewhere. The forces resulting from the proceeding capillary liquid bridge forces (shown as Fig.S1a in Supporting Information), although an order of magnitude smaller (~10^{-8} N) can also be calculated using eq. (3) [47]:

$$Fc_{LB} = \Delta P_c \pi r_2^2 - 2\pi r_2 \gamma_{w/a} \tag{3}$$

where ΔP_c is the pressure difference between the outside and the inside of the liquid bridge and r_2 is the radius of the liquid bridge depicted in Fig.S1b (see Supporting Information). These forces are large enough to lead to further particle deformation. Table S1 in supporting information presents the parameters and estimates of the various forces acting on the particles during film formation.

15

The deformation of particles is highly dependent on temperature through alteration of the rheological response of viscoelastic polymers. Routh and Russel[48] modelled the effect of temperature on the deformation mechanism and the time for complete deformation of latex particles. They showed that if the drying takes place at a temperature below yet near the Tg, the deformation mechanism is governed by either 'dry' or 'moist sintering'. During "dry sintering", the dry latex particles flatten together, with the driving force provided by the surface free energy of the polymer–air interface, while "moist sintering", occurs because of the presence of residual water rings. Regardless of the mechanism leading to the deformation, dry or moist sintering is dominant for less than 15% of the deformation process. For a drying temperature significantly higher than the T_g, "wet sintering," driven by the surface tension between the particles and the solvent, dominates the deformation mechanism.

Visschers *et al.*[47] calculated and compared the capillary forces acting on a particle that has undergone differing amounts of deformation. They noticed that the capillary forces are slightly lower for deformed particles *versus* non-deformed particles. However, it is clear from our studies that plasticized particles undergo markedly larger deformations than unplasticized. This is explained as follows. For example, the plasticized composite containing SWNTs was dried at room temperature, 2 °C above the T_g. Under these conditions, according to the process map of Routh and Russel, the particles will deform by a combination of capillary pressure and wet sintering.[48] At temperatures above T_g, the particles have sufficiently low viscosity to ensure particle deformation within the drying period. Substituting a non-ionic surfactant for an anionic one significantly changes the particles' mechanical properties. The T_g of the unplasticized composite is increased to 31 °C, and the drying is performed 10 °C below the T_g, such that the deformation is governed by dry sintering mechanism. The rate of particle deformation is limited by the high polymer viscosity.

4.3. The magnitude of forces needed to bend a carbon nanotube around a polymer particle

As we have highlighted in the previous section, as the film forms, at each contact surface between

particles there is a localized distribution of both compressive and tensile stresses resulting from capillarity. In order to bend CNTs around the particles, thus creating a connected and continuous CNT network, the superposition of forces must be large enough to overcome the CNT's resistance to bending. The force that is required to bend a CNT around a polymer particle can be roughly approximated using classical mechanics.[49] In this approximation, a CNT is considered as a beam supported at two outer points (points of capillary forces compressing two particles together) and subjected to a concentrated load which is applied perpendicular to the middle of the beam (see discussion in the Supporting Information). Schematic representation of the capillary forces acting on a CNT during latex film formation is shown in Figure 4. If one approximates the Young's modulus of an individual CNT to be ~ 1 TPa (the Young's modulus of CNTs reported in the literature both measured experimentally and estimated theoretically immensely varies from 0.23 to 4.15 TPa.[50-58]) the force needed to bend a CNT around the polymer particles is of the order of 10^{-8} N (using Eq. S2 and associated arguments in the Supporting Information). This is approximately the same order of magnitude as the capillary force generated by the presence of liquid bridges, calculated in the previous section.
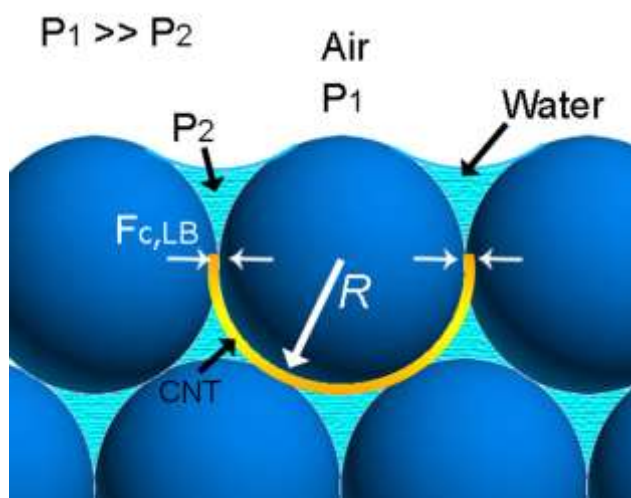

Figure 4. Schematic representation of the pressure difference across the surface of a layer of drying latex and capillary forces acting on a CNT during latex film formation

Consequently, it can be concluded that the capillary forces due to the receding water/air interface are large enough to cause the CNT bending around the polymer particles. Depending on the type of CNT, their fabrication method, the kind and density of defects, the measured bending modulus ranges from 1 GPa to 1 TPa.[59-64] The bending modulus of a CNT rope roughly corresponds to the Young's modulus for a small bundle but strongly decreases with increasing diameter of rope.[65, 66] This is due to the nanotubes in a large bundle acting as a loose assembly of tubes which upon deformation can slip along each other. For example, the bending modulus of a bundle 15 nm in diameter is as low as 100 GPa. [66, 67]

To provide an indication of the extent of CNT de-bundling, Figure 5 (a to c) shows representative AFM images of SWNTs, MWNTs, and DWNTs, respectively, spin-coated onto a mica-sheet from the non-ionic surfactant Triton X-100 based dispersions. Due to the large weight concentration of CNTs (1 mg/ml) dispersed in the all-aqueous dispersions, it is expected that they will consist of large bundles stabilised by surfactant molecules, rather than individually dispersed nanotubes.

SWNTs (Figure 5a) form bundles with the mean diameter of 7 nm that are highly entangled but well dispersed. The assemblies of MWNTs are 6 nm in diameter and exhibit microstructural similarities to SWNTs, as they are also arranged in the form of entangled networks (Figure 5b). Based on these AFM observations, however, DWNTs do not appear to bundle as much as the other types of CNTs and have a mean diameter of 2.5 nm (Figure 5c). The AFM investigations of SWNTs, MWNTs and DWNTs dispersed in water with the assistance of either the anionic SDS or the cationic CTAB surfactants gave similar results (not shown here) to that which is shown in Figure 5 (a to c) for CNTs stabilized with Triton X-100. However, quantitative analysis of length and diameter distribution for the dispersions was not performed.

Based on the observations above, the following conclusion can be drawn. Capillary forces develop when the particles are drying. These forces are strong enough to bend CNTs. However, the nature of bending will be highly dependent on their flexural rigidity dictated by the size of the bundles, such as shown in Figure 5 (d to e). Although, the capillary forces for plasticized and unplasticized particles are

of the same order of magnitude, the plasticized latex particles will undergo significant deformation while the unplasticized particles will remain roughly spherical. Since the capillary forces are very similar for both systems, the CNTs will be bent by the same amount. However, during the evaporation of water the capillary forces acting on particles decrease as a function of drying time. Once the evaporation of water is complete, the capillary forces tend to zero magnitude. It has been shown in the literature that CNTs can be bent elastically and repetitively[68, 69]. As such, regardless of the method used to bend a CNT, when the applied force is removed, they return to their original shape in a spring-like manner. As described in section 4.2, the film formation of the unplasticized particles occurs via dry/moist sintering. Upon completion of the drying process, there is no capillary pressure acting on the particles, and the CNTs will spring back to their original rod-like shape, resulting in the disordered structure shown in Figure 1(d to f). On the other hand, film formation via "wet sintering" takes place for the plasticized particles, resulting in increased particle contact enabling interdiffusion of the particles to fuse around the CNTs. Hence, when the capillary forces disappear, the fused particles will hold the bent CNTs in their positions, thereby preventing them from reverting back to their original configuration. As a result, the CNTs are templated into highly ordered structures as shown in Figure 1(a to c).

It should also be noted that as there is an effective threshold force required to bend the CNTs around the polymer particles; in essence, they are acting like local pressure gauges. This may prove an important observation, as until now, it has been most difficult to experimentally verify theoretical predictions of the magnitude of capillary forces during latex film formation. Moreover, by careful choice of nanostructured fillers with systematic variation in their associated bending modulus, one could precisely measure such capillary forces in a future study. Conversely, systems with known and varying capillary forces could be used to determine the elastic modulus of carbon nanotubes and nanowires.
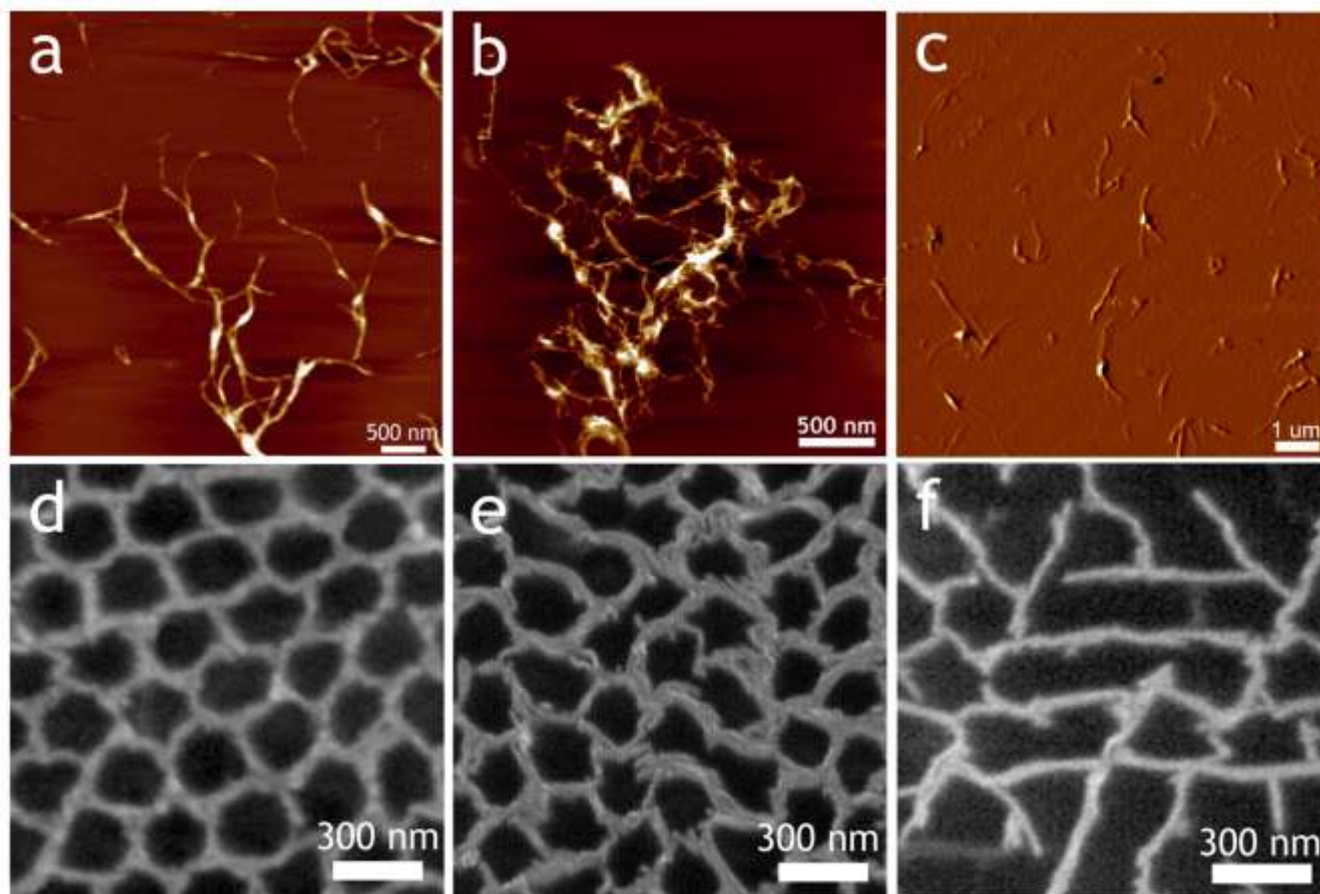
Figure 5. AFM height images of CNTs dispersed in water by means of non-ionic surfactant Triton X-100 and spin-coated onto a mica sheet: (a) SWNTs, (b) MWNTs, (c) DWNTs. SEM micrographs of composites containing (d) SWNT, (e) MWNT and (f) DWNTs with post-added non-ionic surfactant Triton X-100 showing the difference in the flexural rigidity influencing their ability to deform elastically around polymer particles.

5. Conclusions

In summary, we showed that the capillary forces at progressive stages of evaporative self-assembly of colloidal particles are strong enough to bend CNTs (and potentially any nanowire or nanotube with the requisite mechanical properties) around the particles. The understanding and manipulation of these interfacial forces has allowed for the controlled assembly of carbon nanotubes into ordered honeycomb arrangements. The ordering is highly dependent on the type of surfactant used to stabilise the dispersion

in the initial liquid state. The way that the CNTs are assembled within the colloidal crystal can be customized by charge interactions and varying the extent of plasticization by surfactants. Our study points to general design rules to be considered to optimize the ordering of nanostructures within such polymer matrices.

Supporting Information Available. Parameters and estimates of the various forces acting on the particles during film formation and the calculation of the force required to bend a CNT around a polymer particle. This material is available free of charge via the Internet at http://pubs.acs.org.

REFERENCES

1. Duan, H.; Berggren, K. K., Directed Self-Assembly at the 10 nm Scale by Using Capillary Force-Induced Nanocohesion. *Nano Letters* 10, (9), 3710-3716.

2. Nikoobakht, B.; Wang, Z. L.; El-Sayed, M. A., Self-Assembly of Gold Nanorods. *The Journal of Physical Chemistry B* **2000,** 104, (36), 8635-8640.

3. Lee, S. H.; Lee, D. H.; Lee, W. J.; Kim, S. O., Tailored Assembly of Carbon Nanostructures: Tailored Assembly of Carbon Nanotubes and Graphene (Adv. Funct. Mater. 8/2011). *Advanced Functional Materials* **2011,** 21, (8), 1329-1329.

4. Tien, J.; Terfort, A.; Whitesides, G. M., Microfabrication through Electrostatic Self-Assembly. *Langmuir* **1997,** 13, (20), 5349-5355.

5. Walker, D. A.; Browne, K. P.; Kowalczyk, B.; Grzybowski, B. A., Self-Assembly of

Nanotriangle Superlattices Facilitated by Repulsive Electrostatic Interactions. *Angewandte Chemie* 122, (38), 6912-6915.

6.   Liu, K.; Zhao, N.; Kumacheva, E., Self-assembly of inorganic nanorods. *Chemical Society Reviews* 40, (2), 656-671.

7.   Maune, H. T.; Han, S.-p.; Barish, R. D.; Bockrath, M.; Goddard, I. I. A.; RothemundPaul, W. K.; Winfree, E., Self-assembly of carbon nanotubes into two-dimensional geometries using DNA origami templates. *Nat Nano* 5, (1), 61-66.

8.   Duggal, R.; Hussain, F.; Pasquali, M., Self-Assembly of Single-Walled Carbon Nanotubes into a Sheet by Drop Drying. *Advanced Materials* **2006,** 18, (1), 29-34.

9.   Ismach, A.; Joselevich, E., Orthogonal Self-Assembly of Carbon Nanotube Crossbar Architectures by Simultaneous Graphoepitaxy and Field-Directed Growth. *Nano Letters* **2006,** 6, (8), 1706-1710.

10.   Papadopoulos, C., Multi-level carbon nanotube architectures formed via directed self-assembly. *Microelectronic Engineering* **2009,** 86, (4-6), 840-843.

11.   Wang, H.; Wang, X.; Li, X.; Dai, H., Chemical self-assembly of graphene sheets. *Nano Research* **2009,** 2, (4), 336-342.

12.   Shen, J.; Hu, Y.; Li, C.; Qin, C.; Shi, M.; Ye, M., Layer-by-Layer Self-Assembly of Graphene Nanoplatelets. *Langmuir* **2009,** 25, (11), 6122-6128.

13.   Choi, W. B.; Chung, D. S.; Kang, J. H.; Kim, H. Y.; Jin, Y. W.; Han, I. T.; Lee, Y. H.; Jung, J. E.; Lee, N. S.; Park, G. S.; Kim, J. M., *Fully sealed, high-brightness carbon-nanotube field-emission display*. AIP: 1999; Vol. 75, p 3129-3131.

14.   Javey, A.; Guo, J.; Wang, Q.; Lundstrom, M.; Dai, H., Ballistic carbon nanotube field-effect

transistors. *Nature* **2003,** 424, (6949), 654-657.

15.   Roberts, M. E.; LeMieux, M. C.; Bao, Z., Sorted and Aligned Single-Walled Carbon Nanotube Networks for Transistor-Based Aqueous Chemical Sensors. *ACS Nano* **2009,** 3, (10), 3287-3293.

16.   Scardaci, V.; Rozhin, A. G.; Hennrich, F.; Milne, W. I.; Ferrari, A. C., Carbon nanotube-polymer composites for photonic devices. *Physica E: Low-dimensional Systems and Nanostructures* **2007,** 37, (1-2), 115-118.

17.   Loi, M. A.; Gao, J.; Cordella, F.; Blondeau, P.; Menna, E.; Bártová, B.; Hébert, C.; Lazar, S.; Botton, G. A.; Milko, M.; Ambrosch-Draxl, C., Nanohybrids for Photonic Devices: Encapsulation of Conjugated Oligomers in Single-Walled Carbon Nanotubes: Towards Nanohybrids for Photonic Devices (Adv. Mater. 14/2010). *Advanced Materials* **2010,** 22, (14), n/a-n/a.

18.   J. N. Coleman; U. Khan; Y. K. Gun'ko, Mechanical Reinforcement of Polymers Using Carbon Nanotubes. *Advanced Materials* **2006,** 18, (6), 689-706.

19.   Wang, T.; Dalton, A. B.; Keddie, J. L., Importance of Molecular Friction in a Soft Polymerâˆ’Nanotube Nanocomposite. *Macromolecules* **2008,** 41, (20), 7656-7661.

20.   Aliev, A. E.; Lee, S. B.; Baughman, R. H.; Zakhidov, A. A., Thermal properties of carbon inverse opal photonic crystals. *Journal of Luminescence* **2006,** 125, (1-2), 11-17.

21.   Zakhidov, A. A.; Baughman, R. H.; Iqbal, Z.; Cui, C.; Khayrullin, I.; Dantas, S. O.; Marti, J.; Ralchenko, V. G., Carbon Structures with Three-Dimensional Periodicity at Optical Wavelengths. *Science* **1998,** 282, (5390), 897-901.

22.   Kim, I.-D.; Rothschild, A.; Yang, D.-J.; Tuller, H. L., Macroporous TiO2 thin film gas sensors obtained using colloidal templates. *Sensors and Actuators B: Chemical* **2008,** 130, (1), 9-13.

23.   Jiang, B.; Tsavalas, J.; Sundberg, D., Measuring the Glass Transition of Latex-Based Polymers

in the Hydroplasticized State via Differential Scanning Calorimetry. *Langmuir* 26, (12), 9408-9415.

24.   Liu, Y.-T.; Zhang, Z.-L.; Zhao, W.; Xie, X.-M.; Ye, X.-Y., Selective self-assembly of surface-functionalized carbon nanotubes in block copolymer template. *Carbon* **2009,** 47, (7), 1883-1885.

25.   Paunov, V. N.; Panhuis, M. I. H., Fabrication of carbon nanotube-based microcapsules by a colloid templating technique. *Nanotechnology* **2005,** 16, (9), 1522-1525.

26.   Correa-Duarte, M. A.; Kosiorek, A.; Kandulski, W.; Giersig, M.; Liz-Marzán, L. M., Layer-by-Layer Assembly of Multiwall Carbon Nanotubes on Spherical Colloids. *Chemistry of Materials* **2005,** 17, (12), 3268-3272.

27.   Grunlan, J. C.; Kim, Y. S.; Ziaee, S.; Wei, X.; Abdel-Magid, B.; Tao, K., Thermal and mechanical behavior of carbon-nanotube-filled latex. *Macromolecular Materials and Engineering* **2006,** 291, (9), 1035-1043.

28.   Jurewicz, I.; King, A. A. K.; Worajittiphon, P.; Asanithi, P.; Brunner, E. W.; Sear, R. P.; Hosea, T. J. C.; Keddie, J. L.; Dalton, A. B., Colloid-Assisted Self-Assembly of Robust, Three-Dimensional Networks of Carbon Nanotubes over Large Areas. *Macromolecular Rapid Communications* **2010,** 31, (7), 609-615.

29.   Jurewicz, I.; Worajittiphon, P.; King, A. A. K.; Sellin, P. J.; Keddie, J. L.; Dalton, A. B., Locking Carbon Nanotubes in Confined Lattice Geometries - A Route to Low Percolation in Conducting Composites. *The Journal of Physical Chemistry B* **2011,** 115, (20), 6395-6400.

30.   Tzitzinou, A.; Keddie, J. L.; Geurts, J. M.; Peters, A. C. I. A.; Satguru, R., Film Formation of Latex Blends with Bimodal Particle Size Distributions: Consideration of Particle Deformability and Continuity of the Dispersed Phase. *Macromolecules* **2000,** 33, (7), 2695-2708.

31. Odrobina, E.; Feng, J. R.; Kawaguchi, S.; Winnik, M. A.; Neag, M.; Meyer, E. F.,

Characterization of the miscibility of poly(butyl methacrylate) with a nonylphenol ethoxylate surfactant and with various poly(ethylene glycol) oligomers. *Macromolecules* **1998,** 31, (21), 7239-7247.

32.   Farinha, J. P. S.; Martinho, J. M. G.; Kawaguchi, S.; Yekta, A.; Winnik, M. A., Latex Film Formation Probed by Nonradiative Energy Transfer: Effect of Grafted and Free Poly(ethylene oxide) on a Poly(n-butyl methacrylate) Latex. *The Journal of Physical Chemistry* **1996,** 100, (30), 12552-12558.

33.   Bolze, J.; Horner, K. D.; Ballauff, M., Adsorption of the Nonionic Surfactant Triton X-405 on Polystyrene Latex Particles As Monitored by Small-Angle X-ray Scattering. *Langmuir* **1996,** 12, (12), 2906-2912.

34.   Wang, H.; Zhou, W.; Ho, D. L.; Winey, K. I.; Fischer, J. E.; Glinka, C. J.; Hobbie, E. K., Dispersing Single-Walled Carbon Nanotubes with Surfactants: A Small Angle Neutron Scattering Study. *Nano Letters* **2004,** 4, (9), 1789-1793.

35.   Peigney, A.; Laurent, C.; Flahaut, E.; Bacsa, R. R.; Rousset, A., Specific surface area of carbon nanotubes and bundles of carbon nanotubes. *Carbon* **2001,** 39, (4), 507-514.

36.   Gedde, U. W., *Polymer physics*. Chapman & Hall: London; New York, 1995.

37.   Tsavalas, J. G.; Sundberg, D. C., Hydroplasticization of Polymers: Model Predictions and Application to Emulsion Polymers. *Langmuir* **2010,** 26, (10), 6960-6966.

38.   Jiang, B.; Tsavalas, J.; Sundberg, D., Measuring the Glass Transition of Latex-Based Polymers in the Hydroplasticized State via Differential Scanning Calorimetry. *Langmuir* **2010,** 26, (12), 9408-9415.

39.   Soleimani, M.; Haley, J. C.; Lau, W.; Winnik, M. A., Effect of Hydroplasticization on Polymer Diffusion in Poly(butyl acrylate-co-methyl methacrylate) and Poly(2-ethylhexyl acrylate-co-tert-butyl methacrylate) Latex Films. *Macromolecules* **2009,** 43, (2), 975-985.

40.   Tuncel, A.; Kahraman, R.; Piskin, E., Monosize Polystyrene Latices Carrying Functional-Groups on Their Surfaces. *J Appl Polym Sci* **1994,** 51, (8), 1485-1498.

41.   Fukuhara, D.; Sundberg, D., The role of carboxylic acid comonomers in morphology control of synthetic latex particles - batch reactions. *Aqueous Polymer Dispersions* **2004,** 124, 18-21

170.

42.   Brown, W.; Zhao, J., Adsorption of sodium dodecyl sulfate on polystyrene latex particles using dynamic light scattering and zeta potential measurements. *Macromolecules* **1993,** 26, (11), 2711-2715.

43.   Brown, W.; Zhao, J., Interactions between Sodium Dodecyl Sulfate and Styrene-Butadiene Copolymer Latex Particles with Carboxyl Groups Studied Using Dynamic Light Scattering and Electrophoretic Mobility Measurements. *Langmuir* **1994,** 10, (10), 3395-3401.

44.   Becher, P., *Encyclopedia of emulsion technology*. M. Dekker: New York, 1983.

45.   Somasundaran, P., *Encyclopedia of surface and colloid science*. Taylor & Francis, New York: New York, 2006.

46.   Keddie, J. L.; Routh, A. F., *Fundamentals of latex film formation : processes and properties*. Springer: Berlin, 2010.

47.   Visschers, M.; Laven, J.; van der Linde, R., Forces operative during film formation from latex dispersions. *Prog Org Coat* **1997,** 31, (4), 311-323.

48.   Routh, A. F.; Russel, W. B., A Process Model for Latex Film Formation: Limiting Regimes for Individual Driving Forces. *Langmuir* **1999,** 15, (22), 7762-7773.

49.   Gere, J. M.; Timoshenko, S., *Mechanics of materials*. PWS-Kent Pub. Co.: Boston, 1990.

50.   Cho W.S, T., Bending and shear moduli of single-walled carbon nanotubes. *Finite Elements in*

Analysis and Design **2006,** 42, (5), 404-413.

51.   Iijima, S.; Brabec, C.; Maiti, A.; Bernholc, J., Structural flexibility of carbon nanotubes. *The Journal of Chemical Physics* **1996,** 104, (5), 2089-2092.

52.   Tombler, T. W.; Zhou, C.; Alexseyev, L.; Kong, J.; Dai, H.; Liu, L.; Jayanthi, C. S.; Tang, M.; Wu, S.-Y., Reversible electromechanical characteristics of carbon nanotubes under local-probe manipulation. *Nature* **2000,** 405, (6788), 769-772.

53.   Krishnan, A.; Dujardin, E.; Ebbesen, T. W.; Yianilos, P. N.; Treacy, M. M. J., Young's modulus of single-walled nanotubes. *Physical Review B* **1998,** 58, (20), 14013-14019.

54.   Molina, J. M.; Savinsky, S. S.; Khokhriakov, N. V., A tight-binding model for calculations of structures and properties of graphitic nanotubes. *The Journal of Chemical Physics* **1996,** 104, (12), 4652-4656.

55.   Treacy, M. M. J.; Ebbesen, T. W.; Gibson, J. M., Exceptionally high Young's modulus observed for individual carbon nanotubes. *Nature* **1996,** 381, (6584), 678-680.

56.   Salvetat, J. P.; Bonard, J. M.; Thomson, N. H.; Kulik, A. J.; Forró, L.; Benoit, W.; Zuppiroli, L., Mechanical properties of carbon nanotubes. *Applied Physics A: Materials Science & Processing* **1999,** 69, (3), 255-260.

57.   Yu, M.-F.; Lourie, O.; Dyer, M. J.; Moloni, K.; Kelly, T. F.; Ruoff, R. S., Strength and Breaking Mechanism of Multiwalled Carbon Nanotubes Under Tensile Load. *Science* **2000,** 287, (5453), 637-640.

58.   Sears, A.; Batra, R. C., Macroscopic properties of carbon nanotubes from molecular-mechanics simulations. *Physical Review B* **2004,** 69, (23), 235406.

59.   Kalamkarov, A. L.; Georgiades, A. V.; Rokkam, S. K.; Veedu, V. P.; Ghasemi-Nejhad, M. N.,

Analytical and numerical techniques to predict carbon nanotubes properties. *International Journal of Solids and Structures* **2006,** 43, (22-23), 6832-6854.

60.   Gao, R.; Wang, Z. L.; Bai, Z.; de Heer, W. A.; Dai, L.; Gao, M., Nanomechanics of Individual Carbon Nanotubes from Pyrolytically Grown Arrays. *Physical Review Letters* **2000,** 85, (3), 622-625.

61.   Ciocan, R.; Gaillard, J.; Skove, M. J.; Rao, A. M., Determination of the Bending Modulus of an Individual Multiwall Carbon Nanotube using an Electric Harmonic Detection of Resonance Technique. *Nano Letters* **2005,** 5, (12), 2389-2393.

62.   Poncharal, P.; Wang, Z. L.; Ugarte, D.; de Heer, W. A., Electrostatic Deflections and Electromechanical Resonances of Carbon Nanotubes. *Science* **1999,** 283, (5407), 1513-1516.

63.   Lee, K.; Lukic, B.; Magrez, A.; Seo, J. W.; Briggs, G. A. D.; Kulik, A. J.; Forro, L., Diameter-Dependent Elastic Modulus Supports the Metastable-Catalyst Growth of Carbon Nanotubes. *Nano Letters* **2007,** 7, (6), 1598-1602.

64.   Srivastava, D.; Wei, C.; Cho, K., Nanomechanics of carbon nanotubes and composites. *Applied Mechanics Reviews* **2003,** 56, (2), 215-230.

65.   Kis, A.; Csanyi, G.; Salvetat, J. P.; Lee, T.-N.; Couteau, E.; Kulik, A. J.; Benoit, W.; Brugger, J.; Forro, L., Reinforcement of single-walled carbon nanotube bundles by intertube bridging. *Nat Mater* **2004,** 3, (3), 153-157.

66.   Salvetat, J.-P.; Briggs, G. A. D.; Bonard, J.-M.; Bacsa, R. R.; Kulik, A. J.; Stockli, T.; Burnham, N. A.; Forro³, L. s., Elastic and Shear Moduli of Single-Walled Carbon Nanotube Ropes. *Physical Review Letters* **1999,** 82, (5), 944-947.

67.   Ajayan, P. M.; Banhart, F., Nanotubes: Strong bundles. *Nat Mater* **2004,** 3, (3), 135-136.

68.   Knechtel, W. H.; Dusberg, G. S.; Blau, W. J.; Hernandez, E.; Rubio, A., Reversible bending of

carbon nanotubes using a transmission electron microscope. *Applied Physics Letters* **1998,** 73, (14), 1961-1963.

69.   Falvo, M. R.; Clary, G. J.; Taylor, R. M.; Chi, V.; Brooks, F. P.; Washburn, S.; Superfine, R., Bending and buckling of carbon nanotubes under large strain. *Nature* **1997,** 389, (6651), 582-584.